Asian Journal of Chemistry; Vol. 37, No. 4 (2025), 771-778

ASIAN JOURNAL OF CHEMISTRY

https://doi.org/10.14233/ajchem.2025.32722

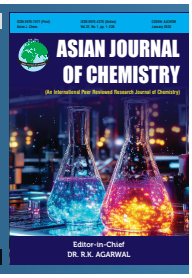

Activated Carbon Synthesized from *Nypa fruticans* and *Areca catechu* by Microwave Method as Efficient Adsorbent for the Removal of Chloramphenicol

BICH NGOC HOANG[1,*], KHA DOANH NGUYEN[2], THI QUE MINH DOAN[1], TRAN THI TUU[1], PHUNG CHI SY[1], LAM VAN TAN[3] and THI CAM QUYEN NGO[1,*]

[1]Institute of Applied Technology and Sustainable Development, Nguyen Tat Thanh University, Ho Chi Minh City 700000, Vietnam
[2]Faculty of Chemical Engineering and Food Technology, Nong Lam University, Ho Chi Minh City 700000, Vietnam
[3]Ben Tre's Department of Science and Technology, Ben Tre Province 86000, Vietnam

*Corresponding authors: E-mail: bichhn@ntt.edu.vn; ntcquyen@ntt.edu.vn

Received: 16 September 2024; *Accepted*: 12 February 2025; *Published online*: 29 March 2025; AJC-21936

This work employed the microwave-assisted method to prepare activated carbons from the byproducts of *Areca catechu* (ACAC) shells and *Nypa fruticans* (ACNF) nut shells. The results show that the materials have a rough surface like a coral reef and contains the characteristic functional groups such as O-H, C=O, C=C, C-O with an amorphous structure. Surface area and pore size were also evaluated with ACAC of 195.93 $m^2 g^{-1}$ and ACNF of 514.91 $m^2 g^{-1}$. The adsorption isotherms predict the size of the pores as small mesopores. The factors affecting ciprofloxacin adsorption using derived activated carbon were also evaluated. For ACAC, the best optimized adsorption conditions were contact time 90 min, temperature 40 ºC, pH 6, dosage 2 g L^{-1}, concentration 80 mg L^{-1}, whereas for ACNF, the best adsorption conditions were contact time 90 min, temperature 40 ºC, pH 4, dosage 1 g L^{-1}, concentration 80 mg L^{-1}. The results show that activated carbon samples ACAC and ACNF follow the pseudo-second-order (PSO) kinetic model, Elovich kinetic model, Dubinin-Radushkevich (D-R) and Temkin isotherms. The Langmuir model was used to record the maximal adsorption capacities of ACAC and ACNF for ciprofloxacin, which were 57.60 mg g^{-1} and 67.59 mg g^{-1}, respectively. The adsorption process occurs by diffusion with chemisorption interactions on a homogeneous surface for ACAC and heterogeneous surface for ACNF.

Keywords: Activated carbon, Microwave assistance, Chloramphenicol, *Nypa fruticans*, *Areca catechu*.

INTRODUCTION

Antibiotic pollution is one of the pollutants that has a great impact on the life of humans and organisms. Antibiotics have a prolonged decomposition time, and their interaction with food can lead to genetic damage at the cellular level [1,2]. At present, several treatment methods exist such as microbial treatment [3], membrane separation [4], chemical oxidation [5] and photocatalysis [6], *etc*. for addressing environmental contaminants, specifically targeting antibiotics. However, most of the treatment method have its own different advantages and disadvantages. Among the treatment method, adsorption is the most popular method to remove antibiotics due to many advantages such as fast action and high treatment efficiency [7,8]. To achieve good treatment efficiency, adsorbent materials need to have high porosity, ease of fabrication and a surface rich in functional groups [9]. Activated carbon material is considered a typical porous material with an extremely diverse structure that can be used as an adsorbent to remove antibiotics in the environment [10-14]. But the raw materials to develop activated carbon are become prioritized by researchers from the agricultural byproducts.

According to the Food and Agriculture Organization (FAO), the cultivated area and production yield of Arecaceae plants (coconut, oil palm, date palm, areca palm) have increased annually [13]. In Vietnam, varieties from the Arecaceae family grow strongly, including coconut, nipa and areca trees. Although the Arecaceae family tree brings many socio-economic and environmental benefits, the agricultural byproducts release a large amount into the environment [13]. They also generate several environmental issues, including air, water and soil pollution, and promote conditions favourable to the spread of numerous

microbial diseases and mosquito vectors. Over the past decade, byproducts from Arecaceae have attracted the lots of attention. The activated carbon material obtained from Arecaceae family are used for the removal of dyes [15,16], heavy metals [17] and some other toxic materials [13,18]. Palm trees, coconut trees and dates have more scientific publications than other types of trees, however, the potential for byproducts of the Arecaceae family has not been fully exploited.

To take advantage of these agricultural wastes and helps in environmental conservation, researchers are focussing on converting them into activated carbon for use in environmental remediation. Therefore, in this work, the byproducts from nipa palm and areca trees are utilized to make activated carbon by microwave assisted activation method with NaOH to accelerate the synthesis process. The activated carbons are employed to eliminate chloramphenicol, an antibiotic, from the aqueous solution in batch experiments, during which adsorption isotherms, kinetics and other related studies will be performed.

EXPERIMENTAL

Antibiotics chloramphenicol (CAS: 56-75-7), ciprofloxacin (CAS: 85721-33-1), tetracycline (CAS: 60-54-8) and oxytetracycline (CAS: 2058-46-0) were provided by Sigma-Aldrich company (USA). Sodium hydroxide and hydrochloric acid were provided by Xilong Scientific Co., Ltd. company (China). *Nypa fruticans* and *Areca catechu* shells were collected from the local market.

Preparation of activated carbons: The raw materials were washed with water to remove dirt and dried at 100 ºC for 24 h. After drying, the sample was finely ground through a D200 mm mash with a sieve size of 0.85 mm. The initial material sample had a particle size < 0.85 mm. Activated carbons from *Areca catechu* shells and *Nypa fruticans* shells were prepared by chemical activation method with a one-stage activation process [19-22]. The raw material sample (50 g) was mixed with 100 mL of 50% NaOH solution and soaked for 2 h. The sample was then microwaved at 600 W for 3 min. After activation, the sample was washed thoroughly with HCl (1 M) and distilled water to remove excess NaOH. The sample was then dried at 100 ºC for 48 h. Activated carbon from *Areca catechu* shells (ACAC) and *Nypa fruticans* shells (ACNF) were finally stored in a desiccator at room temperature.

Characterization: The surface morphology of ACAC and ACNF was observed using a scanning electron microscope (S4800, Japan). Characterization of functional groups present in the structure and on the surface of the material was analyzed using a Nicolet 6700 Spectrometer (FTIR) in the range of 4000-400 cm^{-1} (KBr). The crystallinity of the material was determined through X-ray diffraction using a Siemens D5000 diffractometer at a scan rate of 2º min^{-1} (2θ) with Cu*K*α (1.5406 Å) radiation. The surface area and typical pore size of activated carbon were analyzed using the AMI-Sync 400 analysis system from Altamira Instruments using the Static Volumetric Gas Adsorption (SVGA) method. SVGA using N_2 gas adsorption/desorption with 1 cm^3 g^{-1} degas at 150 ºC in 12 h. A UV-Vis spectrophotometer (Metash UV-5100 spectrophotometer) was used to analyze antibiotic concentrations in water samples.

Adsorption experiments: Batch experiments were conducted to evaluate the adsorption capacity of the activated carbons for antibiotics. The implementation process is based on previous research with some modifications [19-21]. Influential parameters like time (0-300 min), temperature (30-60 ºC), pH in solution (pH 2-10), dosage (0.1-3 g L^{-1}) and dye concentration (0-100 mg L^{-1}) were evaluated through the value of adsorption capacity and adsorption efficiency. Initial dye concentration (C_o) and equilibrium dye concentrations (C_f) were determined using a UV-Vis spectrophotometer. The formula for calculating the value of adsorption capacity (q_e) and adsorption efficiency (H%) is as follows:

$$q_e(\text{mg g}^{-1}) = \frac{(C_o - C_f)\ (\text{mg L}^{-1})}{\text{Dosage (g L}^{-1})} \quad (1)$$

$$H\ (\%) = \frac{(C_o - C_f)\ (\text{mg L}^{-1})}{C_o\ (\text{mg L}^{-1})} \quad (2)$$

Zeta potential measurements (pH_{pzc}): The pH point zero charge (pH_{pzc}) was measured as reported method with little modification [23,24]. Activated carbon (0.1 g) and KCl solution (0.1 mol/L) were mixed in an Erlenmeyer flask with different pH values ranged from 2 to 10. The samples were shaken for 3 h and left to stabilize for 24 h at room temperature. The pH values were recorded initial pH (pH_i) and pH final (pH_f) by using a Hanna Instruments HI2210-02 benchtop pH meter. The pH_{pzc} was determined at the intersection between pH_i and pH_f on the pH value chart [25-27].

Adsorption kinetics and isotherm models: Kinetic and isothermal models are implemented from the equations in the form of nonlinear models. The equations and formulas used are based on the Quyen's research [20]. The models like pseudo-first-order (PFO), pseudo-second-order (PSO), Evlovich and Bangham were used to evaluate the adsorption kinetics [24,29]. The models including Langmuir, Freundlich, Dubinin-Radushkevich (D-R) and Temkin were used to evaluate adsorption isotherms [24]. The coefficients of the each models were calculated along with the adjusted R^2 coefficient and the formulae are presented in Table-1.

RESULTS AND DISCUSSION

Preparation and characterization of activated carbons: The surface morphological features of ACAC and ACNF activated samples were observed by SEM characterization using X500 magnification. At 50 µm in size, ACAC and ACNF were showed a rough surface with the same shape as a coral reef (Fig. 1). It can be seen that the pores of ACNF are larger than ACAC material. The uniform distribution of regular pores and mesopores across the surface of carbon particles, which is agreement with the reported work [30]. The porous structure was formed through the activation of NaOH under microwave-assisted method. The influence of NaOH promoted dehydration and decomposition reactions during the early phase of activation, enhancing the development of surface morphological structures. The activation process of NaOH in lignocellulose produced the first product Na_2CO_3 [9]. In the next step, Na_2CO_3 was removed through the washing process with HCl and water.

TABLE-1
EQUATIONS OF KINETIC AND ISOTHERMAL MODELS

Adsorption isotherm			Adsorption kinetics		
Model name	Equation	Ref.	Model name	Equation	Ref.
Langmuir	$q_e = \frac{q_m K_L C_e}{1 + K_L C_e}$ $\left(R_L = \frac{1}{1 + K_L C_o}\right)$	[20]	Pseudo–first–order (PFO)	$q_t = q_e(1 - e^{-k_1 t})$	[20]
Freundlich	$q_e = K_F C_e^{1/n}$	[20]	Pseudo–second–order (PSO)	$q_t = \frac{q_e^2 k_2 t}{1 + k_2 t q_e}$	[20]
Dubinin-Radushkevich (DR)	$q_e = q_m e^{-BE^2}$ $\left\{E = \frac{1}{\sqrt{2B}}; \varepsilon = RT \ln\left(1 + \frac{1}{C_e}\right)\right\}$	[20]	Bangham	$q_t = k_B t^{\alpha_B}$	[20]
Temkin	$q_e = B_T \ln(K_T C_e)$ $\left(B_T = \frac{RT}{b}\right)$	[20]	Evlovich	$q_t = \frac{1}{\beta} \ln(1 + \alpha\beta t)$	[20]

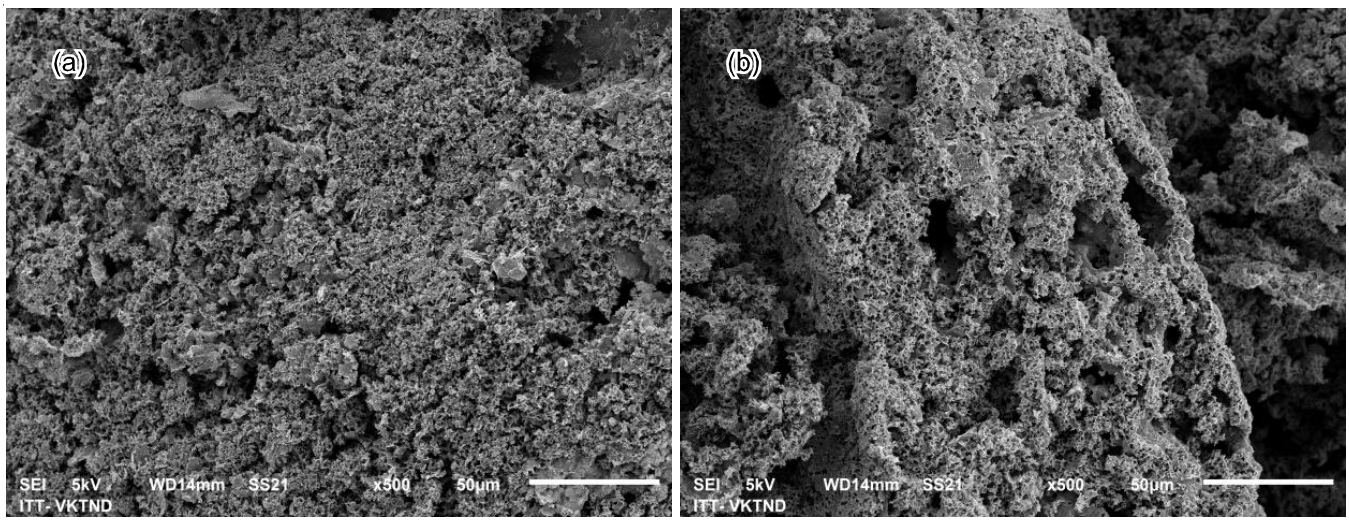

Fig. 1. SEM images of ACAC (a) and ACNF (b) materials

FTIR studies: The functional groups on the surface of ACAC and ACNF materials were predicted through FTIR analysis. The stretch and broad vibration from peak 3700-3200 cm^{-1} is due to -OH bonding of the alcohol/phenol group. This is attributed to the appearance of free hydroxyl groups and hydrogen bonds on the surface. Peak 2875 and 1450 cm^{-1} with a small vibration represents the C-H bond of the alkane group (Fig. 2). Peaks at 1650 cm^{-1} with stretch and average vibration represented the C=O bonding of the amide group. The peaks at 1320-1000 cm^{-1} are believed to be the stretching and asymmetric vibrations of C-O, C-O-C bonding of alcohols, carboxylic acids, esters and ethers related to cellulose, hemicellulose and aromatic rings. The absorption bands around 1380 cm^{-1} are attributed to the C=C stretching and bending vibration, respectively. The peaks at 780 cm^{-1} in the FT-IR spectrum for raw carbon disappeared for activated carbons. The peaks at around 1120, 780 and 470 cm^{-1} in the FT-IR spectra disappeared for ACs, probaby due to chemical activation, which enhanced the strength and aromaticity of carbon structure [28].

XRD studies: The activation process has resulted in the formation of pores on the surface due to the alterations in the original structure of ACAC and ACNF adsorbents. The BET equation was used to determine the surface area of the material based on the nitrogen gas adsorption/desorption process. The

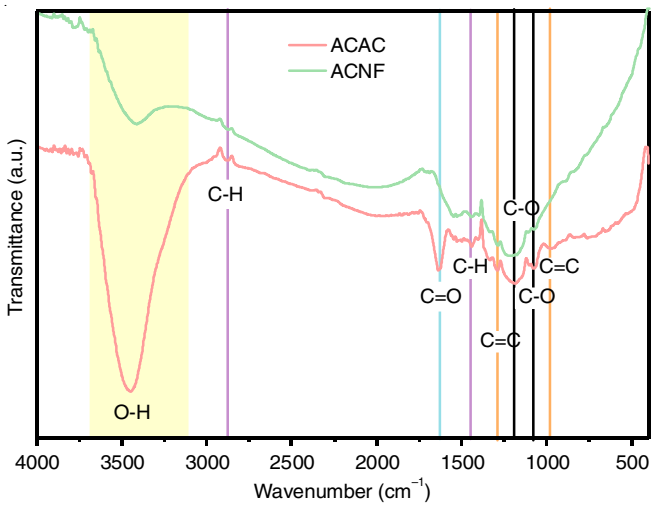

Fig. 2. FTIR spectra of ACAC and ACNF adsorbents

XRD results and nitrogen adsorption/desorption isotherms are shown in Fig. 3. The XRD patterns show two main broad peaks identified near 2θ = 24° (ACAC), 29° (ACNF) and 2θ = 42° (ACAC & ACNF) due to reflections from the (002) and (100) planes, respectively. Therefore, the XRD patterns reveal that the both activated carbons possess an amorphous structure [29].

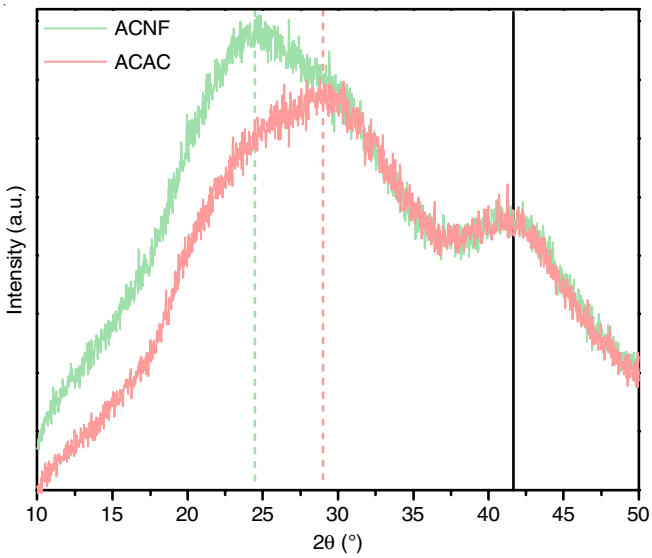

Fig. 3. XRD spectra of ACAC and ACNF adsorbents

Nitrogen adsorption/desorption isotherm studies: According to the IUPAC classification, samples ACNF and ACAC had an adsorption isotherm of type IV with a hysteresis loop of type H4 [30]. The values at $P/P_o \sim 0.4$ showed the presence of small mesopores (Fig. 4) [30]. The main characteristic of the type IV isotherm is the occurrence of capillary condensation within pores. The initial segment of the type IV isotherm is linked to the transition from monolayer to multilayer adsorption, similar to the behavior observed in the type II isotherm [31]. Hysteresis represents the capillary condensation in the mesopores and macropores.

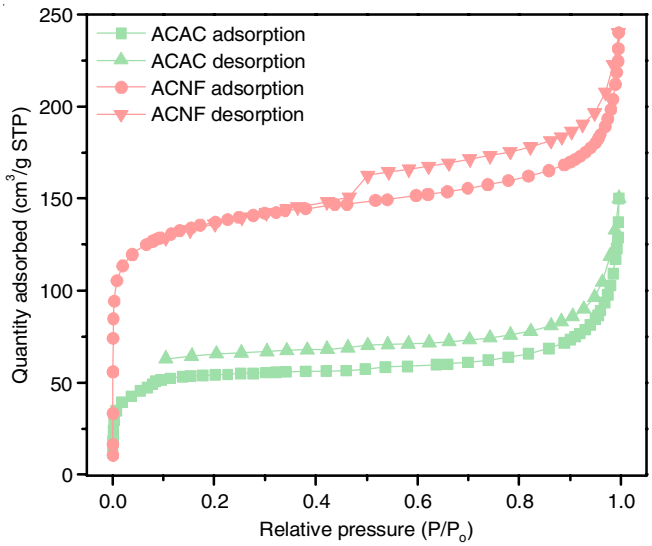

Fig. 4. N_2 adsorption/desorption isotherms of ACAC and ACNF adsorbents

Parameters such as surface area, pore volume and pore size are shown in Table-2. The specific surface areas of ACAC and ACNF were found to be 195.93 $m^2 g^{-1}$ and 514.91 $m^2 g^{-1}$ after NaOH activation. The pore sizes and volume of ACAC and ACNF range from 2.64-3.92 nm and 0.34-0.19 $cm^3 g^{-1}$, respectively. These results corresponded with Lalhmunsiama's study on activated carbon obtained from Areca [31] and Farma's study of activated carbon obtained from Nipa palm trees [32].

TABLE-2
THE PARAMETERS OF SURFACE AREA, PORE VOLUME AND PORE SIZE

Parameters	ACAC	ACNF
Surface area ($m^2 g^{-1}$)	195.93	514.91
Pore volume ($cm^3 g^{-1}$)	0.19	0.34
Pore size (nm)	3.92	2.64

Adsorption studies: A preliminary assessment for the removal of different antibiotics such as chloramphenicol (CPR), ciprofloxacin (CFX), tetracycline (TCC) and oxytetracycline (OTC) was conducted by utilizing ACAC and ACNF adsorbents. For CPR antibiotic, the ACAC gave a higher adsorption capacity of 20.2 mg g^{-1} as compared to other studied antibiotics for the evaluation. For ACNF, CPR and TCC antibiotics reached 19.6 mg g^{-1} and 19.2 mg g^{-1}, respectively. It can be seen (Fig. 5) that CPR antibiotic give the best adsorption capacity for both activated carbons. Therefore, CPR antibiotic was chosen to evaluate the further experiments.

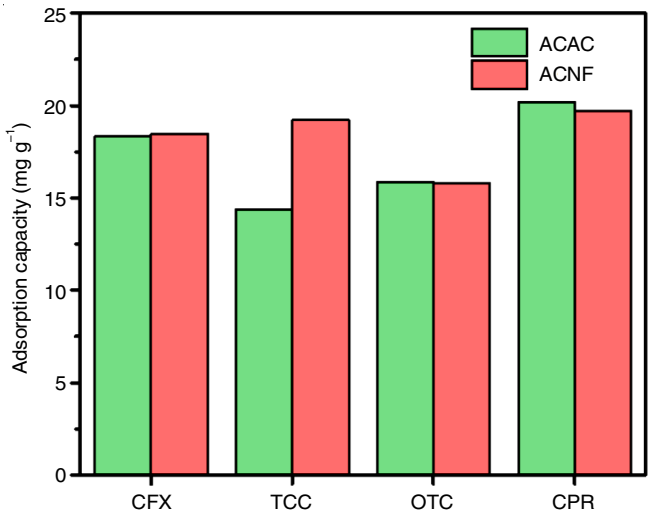

Fig. 5. Adsorption efficiencies of ACAC and ACNF towards different antibiotics

Optimization parameters of CPR antibiotic adsorption

The adsorption process is the interaction between the adsorbent and the adsorbed materials and influencing not only by interaction forces but also surrounding factors. Therefore, the evaluation of influencing factors was carried out including adsorption time, pH in solution, temperature, charcoal dosage and antibiotic concentration. Time and temperature factors were evaluated and shown in Fig. 6. Based on Fig. 6a, the adsorption process takes place quickly from 0 to 10 min, reaching an adsorption capacity of 11.7 mg g^{-1}. The adsorption process gradually decreased from 10 to 60 min with the adsorption capacity increasing from 11.6 to 16.3 mg g^{-1}. The adsorption process achieves saturation, with the capacity stabilizing at 18 mg g^{-1} by 240 min.

The influence of temperature was evaluated in the range of 30-60 ºC. Adsorption capacity was increased when increasing the temperature from 30 to 40 ºC and recorded the values from 16 to 18.5 mg g^{-1} (Fig. 6b). When the temperature was

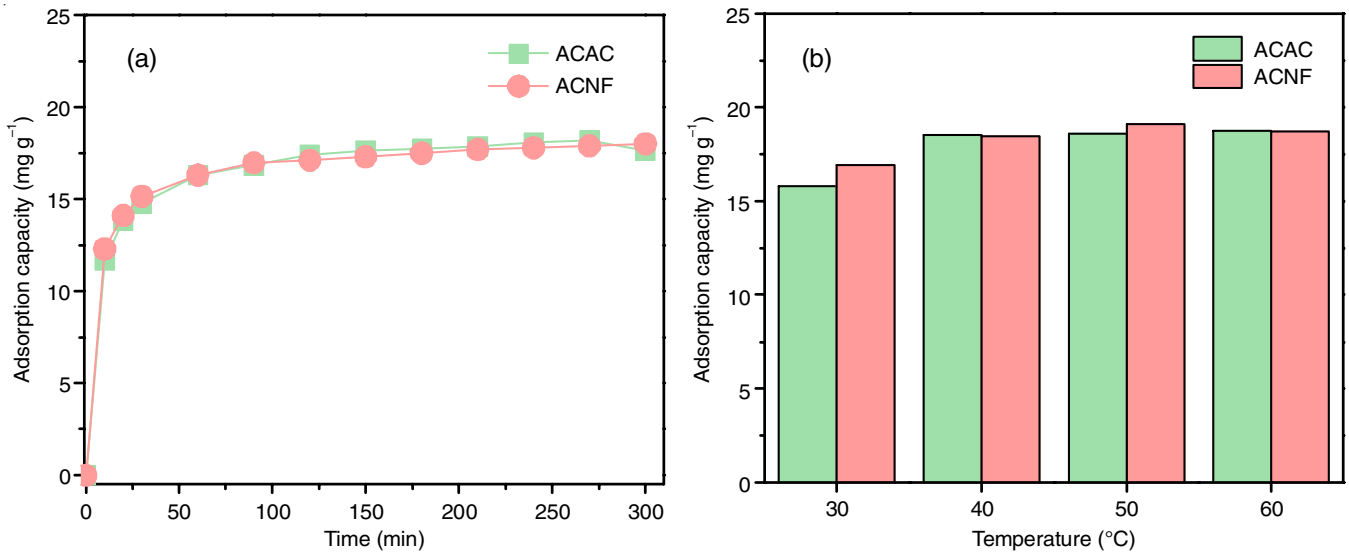

Fig. 6. Effect of time (a) and temperature (b) of ACAC and ACNF

further increased to 50 and 60 ºC, the adsorption capacity remained almost unchanged and recorded a value of 18.53 mg g^{-1} (ACAC) and 19.11 mg g^{-1} (ACNF). There is not much difference in adsorption capacity, which indicate that ACAC and ACNF materials are less affected by temperature. The adsorption duration for ACAC and ACNF was selected to be 90 min at 40 ºC to reduce expense and operational time.

Effect of pH: The effect of pH was evaluated from pH 2 to 10. In addition, to have a more general view of the effect of pH, the isoelectric point of material (pH_{pzc}) was also analyzed. The results of evaluating the pH and pH_{pzc} of the material are shown in Fig. 7. The adsorption capacity of ACAC and ACNF at pH 4 (Q_{ACAC}= 16.67 mg g^{-1}, Q_{ACNF} = 17.32 mg g^{-1}) and pH 6 (Q_{ACAC} = 16.93 mg g^{-1}, Q_{ACNF} = 16.80 mg g^{-1}) were better than other pHs (Fig. 7a). For ACAC, the pH_{pzc} value was recorded at pH 4.05 and the antibiotic adsorption capacity at pH 6 was better than pH 4. This shows that pH_{pzc} was smaller as the surface of ACAC is positively charged [27,33]. For ACNF, the pH_{pzc} value was recorded at pH 4.25 and the ability to adsorb antibiotic at pH 4 was better than pH 6, which shows that pH_{pzc} was greater as the surface of ACNF is negatively charged [27,33]. The results show that both adsorbents works well in moderately acidic to neutral pH as the pH condition of the solution won't greatly affect the adsorption capacity of activated carbon. Therefore, pH 6 for ACAC and pH 4 for ACNF were chosen to evaluate for further experiments.

Effect of dosage and concentration: It was observed that at the initial stage, increase in the dosage enhanced the adsorption process; however, beyond the optimal condition, further increases in dosage adversely impacted the adsorption process at lower temperatures (Fig. 8). The results showed that at the dosage of 1 g L^{-1} to 3 g L^{-1}, the adsorption efficiency reaches nearly 100%. To achieve an equilibrium between capacity and efficiency, the optimum dosage should be efficiency exceeding 90%. Thus, the optimum dosage is 1 g L^{-1} for ACNF and 2 g L^{-1} for ACAC. Based on Fig. 8b, it was observed that at the intial concentration of 10 till 60 mg L^{-1}, the adsorption process takes place quickly and is almost constant at concentrations from 60 to 100 mg L^{-1}. The adsorption capacity reaches the maximum value of 40.90 mg g^{-1} with ACNF and 37.50 mg g^{-1} with ACAC at 80 mg L^{-1} concentration. Thus, for ACAC, the best adsorption conditions are optimized as time 90 min, temperature 40 ºC, pH 6, dosage 2 g L^{-1}, concentration 80 mg L^{-1}. And for ACNF, the best adsorption conditions are time 90 min, temperature 40 ºC, pH 4, dosage 1 g L^{-1}, concentration 80 mg L^{-1}.

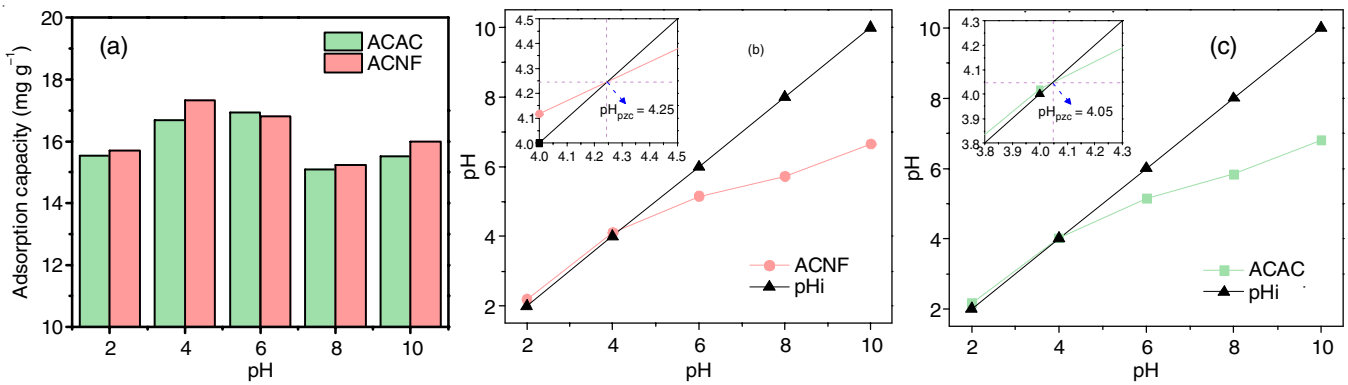

Fig. 7. Effect of pH (a) and pH pzc values (b,c) of ACAC and ACNF

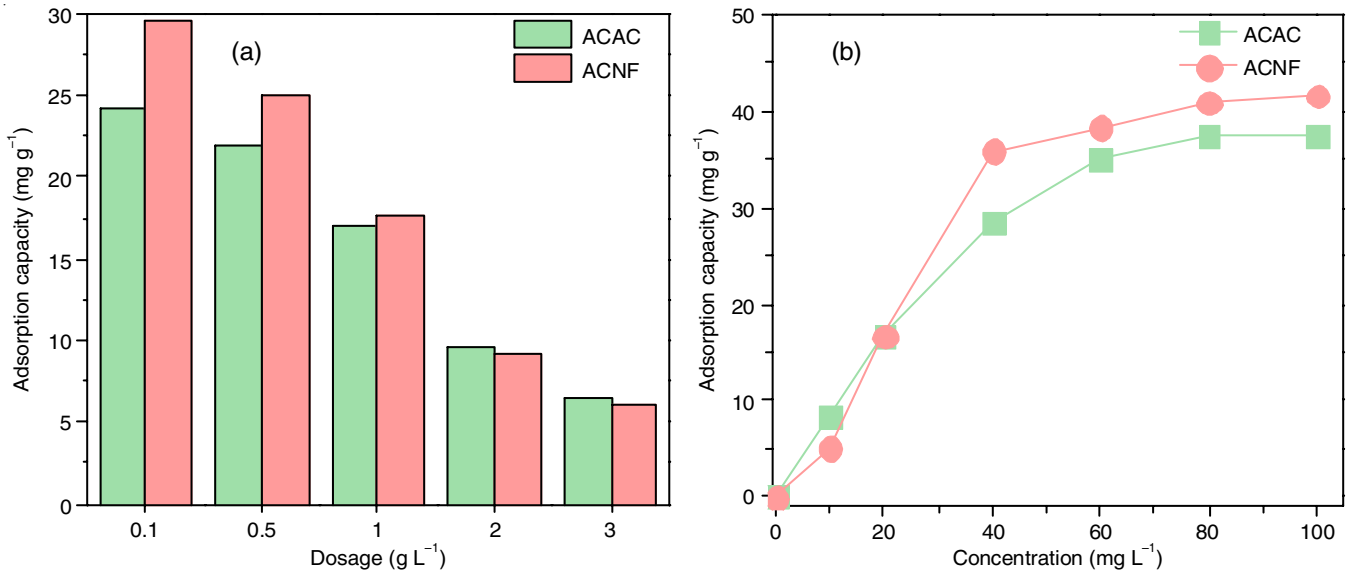

Fig. 8. Effect of dosage of ACAC and ACNF (a) and CPR concentration (b)

Adsorption kinetics and isotherms: The kinetics and adsorption isotherm models were performed based on the selected conditions. The results of the kinetic model are shown in Table-3. The experiments were evenly distributed on the time graph to apply the kinetic equations and calculated related coefficients. The results show that the pseudo-second-order (PSO) model gave a higher correlation coefficient than other models, corresponding to R^2 adjusted = 0.998 (ACNF) and 0.997 (ACAC). Besides, the Elovich model also has a correlation coefficient nearly as high as the PSO model with R^2 adjusted = 0.994 (ACNF) and 0.990 (ACAC). From the kinetic model, it can be seen that the adsorption process follows the chemical adsorption as well as the diffusion mechanisms. The main control process is the chemical adsorption process.

TABLE-3
PARAMETERS OF THE ADSORPTION KINETIC MODEL

Model	Parameter	ACAC	ACNF
Bangham	R^2 adjusted	0.986	0.992
	k_B [mL (g L^{-1})$^{-1}$]	9.95	10.60
	α_B	0.11	0.10
Elovich	R^2 adjusted	0.990	0.994
	α [mg (g min)$^{-1}$]	201.70	643.96
	β (g mg^{-1})	0.56	0.64
Pseudo-first-order	R^2 adjusted	0.973	0.975
	q_e (mg g^{-1})	17.41	17.26
	k_1 (min^{-1})	0.09	0.11
Pseudo-second-order	R^2 adjusted	0.997	0.998
	q_e (mg g^{-1})	18.28	18.00
	k_2 (min^{-1})	0.01	0.01

Chloramphenicol adsorption capacity is controlled by chemical adsorption and diffusion processes, so related parameters include time rate constant (k), adsorption capacity to reach equilibrium (q_e), adsorption (a) and desorption (b) rate coefficient. The rate constant according to the PSO model for both adsorbents are same (Table-3). However, the adsorption and desorption coefficients according to the Elovich model are different. The adsorption coefficient of ACNF (643.96 mg g^{-1} min^{-1} was three times higher than that of ACAC (201.70 mg g^{-1} min^{-1}). But the desorption rates were almost the same: 0.56 g mg^{-1} (ACAC) and 0.64 g mg^{-1} (ACNF), respectively (Fig. 9). Although ACNF has a higher desorption rate, the results demonstrate that it can adsorb more swiftly and greatly than ACAC. This leads to the pores of the ACNF being more quickly filled with antibiotic molecules than ACAC.

The results of four isotherm models are shown in Table-4, which indicate that Temkin model has a high correlation coefficient with ACAC (R^2 adjusted = 0.988). Besides, the D-R model has a high correlation coefficient with ACNF (R^2 adjusted = 0.990). The Temkin model described the adsorption process by interacting between the antibiotic and adsorbent with bonds and energy uniformly distributed on the adsorbent surface [34, 35]. For the D-R model, the adsorption process was described by the interaction of the antibiotic and adsorbent with a Gaussian energy distribution with evaluation conditions such as the size of the antibiotic and pores adsorbent, not affected by tempera-

TABLE-4
PARAMETERS OF THE ADSORPTION ISOTHERM MODEL

Model	Parameter	ACAC	ACNF
DR	R^2 adjusted [(mol^2) (kJ^2)$^{-1}$]	0.955	0.990
	q_m (mg g^{-1})	37.34	43.01
	ε	59.90	95.33
	β	45.77	58.47
	E (kJ mol^{-1})	0.11	0.09
Freundlich	R^2 adjusted	0.954	0.896
	K_F (mg g^{-1})	3.67	3.38
	1/n (min^{-1})	0.53	0.57
Langmuir	R^2 adjusted	0.985	0.941
	q_m (mg g^{-1})	57.60	67.59
	K_L (L mg^{-1})	0.02	0.02
	R_L	0.38	0.38
Temkin	R^2 adjusted	0.988	0.964
	b (J mol^{-1})	191.11	154.36
	B_T	13.61	16.85
	k_T (L mg^{-1})	0.19	0.15

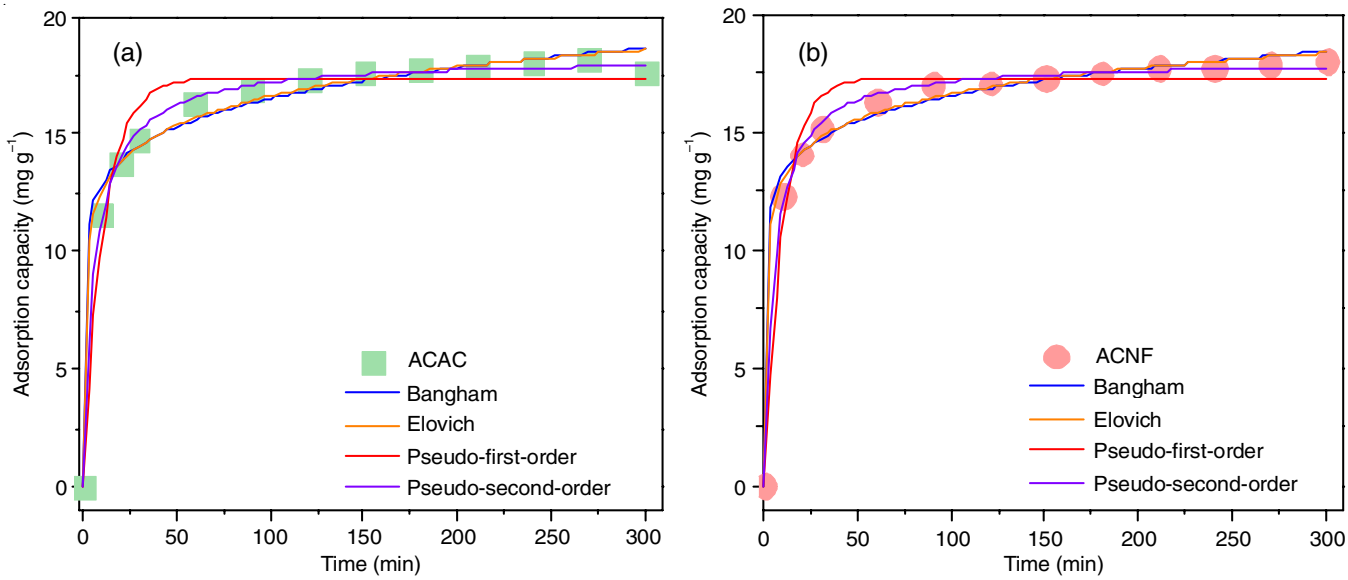

Fig. 9. Kinetic plots fitting of pseudo first order, pseudo second order, Elovich and Bangham diffusion models of ACAC (a) and ACNF (b)

ture [35,36]. From the isothermal model, it can be observed that ACAC had an adsorption mechanism according to uniform energy distribution on the surface. At the same time, ACNF follows a non-uniform Gaussian energy distribution on the surface.

Chloramphenicol adsorption capacity is controlled by Temkin and Dubinin-Radushkevich (D-R) models, so the related parameters like Temkin constant (b), Temkin isotherm constant (k_T), maximum adsorption capacity from the plot (q_m), Polanyi potential (ε), Dubinin-Radushkevich constant (B) and mean adsorption energy (E). For ACAC, Temkin isotherm constant and temkin constant are recorded as b = 191.11 J mol^{-1}, K_t = 0.19 L mg^{-1}, respectively. The results show that the adsorption process model of ACAC wasn't affected by the temperature. For ACNF, the Polanyi potential, Dubinin-Radushkevich constant were and mean adsorption energy were recorded as ε = 95.33, β = 58.47, E = 0.09, respectively, which show that the adsorption process model of ACNF was affected by the temperature (Fig. 10). The maximum adsorption capacities of ACAC and ACNF were recorded from the Langmuir model such as 57.60 and 67.59 mg g^{-1}. The adsorption mechanism in different stages is facilitating the development and exploitation of activated carbon derived from the Arecacae family.

Conclusion

The activated carbon prepared from the byproducts of nipa coconut shells and areca nut shells using the microwave-assisted method. The results show that the material has a rough surface like a coral reef, and consist of the characteristic functional groups such as O-H, C=O, C=C, and C-O with an amorphous structure. For ACAC, the adsorption mechanism is described by a diffusion process with chemisorption interactions on a homogeneous surface. For ACNF, the adsorption mechanism is described by a diffusion process with chemisorption interactions on a heterog-

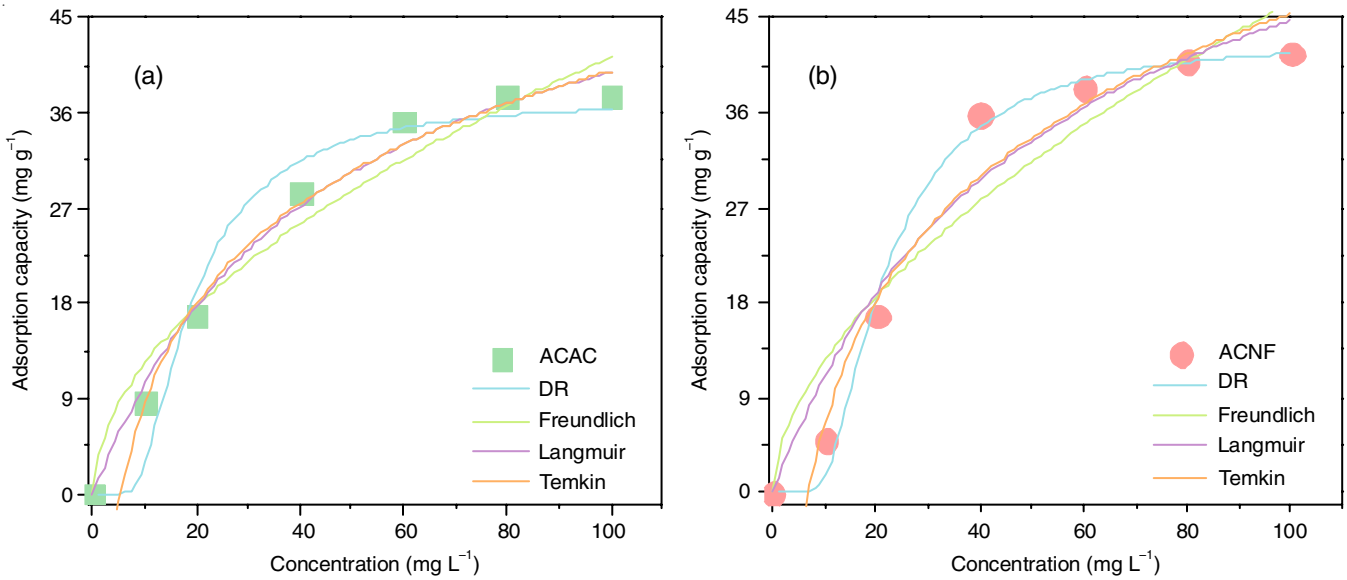

Fig. 10. Isothermal plots fitting of Dubinin-Radushkevich (D-R), Langmuir, Freundlich and Temkin models of ACAC (a) and ACNF (b)

eneous surface. The maximum adsorption capacities of ACAC and ACNF were recorded from the Langmuir model such as 57.60 mg g^{-1} and 67.59 mg g^{-1}. Research results have shown the benefits of activated carbon from areca shells and nipa coconut shells to treat antibiotics from the wastewater.

ACKNOWLEDGEMENTS

This research was fund by a grant from the Science and Technology Development Foundation of Nguyen Tat Thanh University with code (2024.01.122/HĐ-KHCN).

CONFLICT OF INTEREST

The authors declare that there is no conflict of interests regarding the publication of this article.

REFERENCES

1. S.A. Kraemer, A. Ramachandran and G.G. Perron, *Microorganisms*. **7**, 180 (2019); https://doi.org/10.3390/microorganisms7060180
2. J. Kusi, C.O. Ojewole, A.E. Ojewole and I. Nwi-Mozu, *Antibiotics*. **11**, 821 (2022); https://doi.org/10.3390/antibiotics11060821
3. M.S. Islam, Y. Zhang, K.N. McPhedran, Y. Liu and M. Gamal El-Din, *Appl. Environ. Microbiol.*, **81**, 4037 (2015); https://doi.org/10.1128/AEM.04258-14
4. A. Angelakis and S. Snyder, *Water*, **7**, 4887 (2015); https://doi.org/10.3390/w7094887
5. G. Boczkaj and A. Fernandes, *Chem. Eng. J.*, **320**, 608 (2017); https://doi.org/10.1016/j.cej.2017.03.084
6. Z. Wei, J. Liu and W. Shangguan, *Chinese J. Catal.*, **41**, 1440 (2020); https://doi.org/10.1016/S1872-2067(19)63448-0
7. N.F. Anuar, D.R.S.I. Shah, F.F. Ramli, M.S.M. Zaini, N.A. Mohammadi, A.R.M. Daud and S.S.A. Syed-Hassan, *J. Clean. Prod.*, **401**, 136725 (2023); https://doi.org/10.1016/j.jclepro.2023.136725
8. M.W. Nugraha, S. Kim, F. Roddick, Z. Xie and L. Fan, *J. Water Process Eng.*, **70**, 106960 (2025); https://doi.org/10.1016/j.jwpe.2025.106960
9. Z. Heidarinejad, M.H. Dehghani, M. Heidari, G. Javedan, I. Ali and M. Sillanpää, *Environ. Chem. Lett.*, **18**, 393 (2020); https://doi.org/10.1007/s10311-019-00955-0
10. T.C.Q. Ngo, T. Kim Ngan Tran, H. Dung Chau and B. Ngoc Hoang, *Mater. Today Proc.*, (2023); https://doi.org/10.1016/j.matpr.2023.03.511
11. M.F. Hassan, M.A. Sabri, H. Fazal, A. Hafeez, N. Shezad and M. Hussain, *J. Anal. Appl. Pyrolysis*, **145**, 104715 (2020); https://doi.org/10.1016/j.jaap.2019.104715
12. T.K.N. Tran, T.C.Q. Ngo, Q.V. Nguyen, T.S. Do and N.B. Hoang, *Mater. Today: Proc.*, **60**, 1914 (2022); https://doi.org/10.1016/j.matpr.2022.01.020
13. N.B. Hoang, T.C.Q. Ngo, T.K.N. Tran and V.T. Lam, *Open Chem.*, **20**, 10 (2022); https://doi.org/10.1515/chem-2021-0117
14. K.N.T. Tran, T.B. Tran, S.T. Do, K.O.T. Nguyen and T.V. Lam, *Indo. J. Chem.*, **22**, 96 (2022); https://doi.org/10.22146/ijc.67742
15. B.G. Alhogbi, S. Altayeb, E.A. Bahaidarah and M.F. Zawrah, *Processes*, **9**, 416 (2021); https://doi.org/10.3390/pr9030416
16. R.S. Piriya, R.M. Jayabalakrishnan, M. Maheswari, K. Boomiraj and S. Oumabady, *Water Sci. Technol.*, **83**, 1167 (2021); https://doi.org/10.2166/wst.2021.050
17. S. Ravulapalli and R. Kunta, *J. Environ. Chem. Eng.*, **6**, 4298 (2018); https://doi.org/10.1016/j.jece.2018.06.033
18. F.G. de Souza, F.F. de Araújo, D. de Paulo Farias, A.W. Zanotto, I.A. Neri-Numa and G.M. Pastore, *Food Res. Int.*, **138**, 109690 (2020); https://doi.org/10.1016/j.foodres.2020.109690
19. V.T. Lam, B. Hoang and N.T.C. Quyen, *Adv. Sci. Technol.*, **122**, 57 (2023); https://doi.org/10.4028/p-0iyi0c
20. N.T.C. Quyen, T.L. Van, L.G. Bach and B.N. Hoang, *Key Eng. Mater.*, **949**, 175 (2023); https://doi.org/10.4028/p-VfN0Z5
21. N. Van Phuoc, H.L. Quoc, T.T. Tran, L. Van Tan and B.N. Hoang, *J. Chem. Res.*, **47**, 17475198231212143 (2023); https://doi.org/10.1177/17475198231212143
22. L. Zhu, Q. Wang, H. Wang, F. Zhao and D. Li, *Ind. Crops Prod.*, **187(B)**, 115458 (2022); https://doi.org/10.1016/j.indcrop.2022.115458
23. T. Van Tran, Q.T.P. Bui, T.D. Nguyen, V.T.T. Ho and L.G. Bach, *Water Sci. Technol.*, **75**, 2047 (2017); https://doi.org/10.2166/wst.2017.066
24. B. Ngoc Hoang, T. Thi Nguyen, D. Van Nguyen and L. Van Tan, *Mater. Today Proc.*, **38**, 3046 (2021); https://doi.org/10.1016/j.matpr.2020.09.391
25. A. Pal, A. Giri and A. Bandyopadhyay, *J. Environ. Chem. Eng.*, **4**, 1731 (2016); https://doi.org/10.1016/j.jece.2016.02.034
26. M. Kosmulski, *Adv. Colloid Interface Sci.*, **275**, 102064 (2020); https://doi.org/10.1016/j.cis.2019.102064
27. M. Kosmulski, *Adv. Colloid Interface Sci.*, **319**, 102973 (2023); https://doi.org/10.1016/j.cis.2023.102973
28. S. Joshi, R.G. Shrestha, R.R. Pradhananga, K. Ariga and L.K. Shrestha, *J. Carbon Res.*, **8**, 1 (2022); https://doi.org/10.3390/c8010002
29. S. Wang, H. Nam, T.B. Gebreegziabher and H. Nam, *Eng. Rep.*, **2**, e12083 (2020); https://doi.org/10.1002/eng2.12083
30. K.S.W. Sing, *Pure Appl. Chem.*, **57**, 603 (1985); https://doi.org/10.1351/pac198557040603
31. S. Lalhmunsiama, S. Lee, S. Choi and D. Tiwari, *Metals*, **7**, 248 (2017); https://doi.org/10.3390/met7070248
32. R. Farma, I. Apriyani, Awitdrus, M. Deraman, E. Taer, R.N. Setiadi and A.S. Rini, *J. Energy Storage*, **67**, 107611 (2023); https://doi.org/10.1016/j.est.2023.107611
33. S. Raghav and D. Kumar, *J. Chem. Eng. Data*, **63**, 1682 (2018); https://doi.org/10.1021/acs.jced.8b00024
34. R.R. Karri, J.N. Sahu and N.S. Jayakumar, *J. Taiwan Inst. Chem. Eng.*, **80**, 472 (2017); https://doi.org/10.1016/j.jtice.2017.08.004
35. N. Ayawei, A.N. Ebelegi and D. Wankasi, *J. Chem.*, **2017**, 3039817 (2017); https://doi.org/10.1155/2017/3039817
36. X. Chen, *Information*, **6**, 14 (2015); https://doi.org/10.3390/info6010014